Biosensors and Bioelectronics 80 (2016) 590–600

Contents lists available at ScienceDirect

Biosensors and Bioelectronics

journal homepage: www.elsevier.com/locate/bios

# Long period fiber grating nano-optrode for cancer biomarker detection

Giuseppe Quero [a,1], Marco Consales [a,1], Renato Severino [a], Patrizio Vaiano [a], Alessandra Boniello [a], Annamaria Sandomenico [b,c], Menotti Ruvo [b,c,*], Anna Borriello [d,*], Laura Diodato [d], Simona Zuppolini [d], Michele Giordano [d], Immacolata Cristina Nettore [e], Claudia Mazzarella [f], Annamaria Colao [e], Paolo Emidio Macchia [e], Flavio Santorelli [g], Antonello Cutolo [a], Andrea Cusano [a,*]

[a] Optoelectronics Group, Department of Engineering, University of Sannio, Benevento, Italy
[b] Istituto di Biostrutture e Bioimmagini, Consiglio Nazionale delle Ricerche (IBB-CNR), Napoli, Italy
[c] Centro Interuniversitario di Ricerca sui Peptidi Bioattivi (CIRPeB), Napoli, Italy
[d] Institute for Polymers, Composites and Biomaterials (IPCB) -CNR, Portici, Italy
[e] Department of Clinical Medicine and Surgery, University of Napoli "Federico II", Napoli, Italy
[f] Department of Traslational Medicine, University of Napoli "Federico II", Napoli, Italy
[g] Hospital Consulting SpA, Bagno a Ripoli, Firenze, Italy

ARTICLE INFO

*Article history:*
Received 28 October 2015
Received in revised form
27 January 2016
Accepted 8 February 2016
Available online 13 February 2016

*Keywords:*
Optical fiber biosensor
Long period fiber grating (LPG)
Reflection-type LPG
Human Thyroglobulin (TG) detection
Biomolecular sensing
Label-free detection

ABSTRACT

We report an innovative fiber optic nano-optrode based on Long Period Gratings (LPGs) working in reflection mode for the detection of human Thyroglobulin (TG), a protein marker of differentiated thyroid cancer.

The reflection-type LPG (RT-LPG) biosensor, coated with a single layer of atactic polystyrene (aPS) onto which a specific, high affinity anti-Tg antibody was adsorbed, allowed the label-free detection of Tg in the needle washouts of fine-needle aspiration biopsies, at concentrations useful for pre- and post-operative assessment of the biomarker levels.

Analyte recognition and capture were confirmed with a parallel on fiber ELISA-like assay using, in pilot tests, the biotinylated protein and HRP-labeled streptavidin for its detection. Dose-dependent experiments showed that the detection is linearly dependent on concentration within the range between 0 and 4 ng/mL, while antibody saturation occurs for higher protein levels. The system is characterized by a very high sensitivity and specificity allowing the *ex-vivo* detection of sub ng/ml concentrations of human Tg from needle washouts of fine-needle aspiration biopsies of thyroid nodule from different patients.



## 1. Introduction

The ever increasing incidence of cancer diseases is imposing the development of highly sensitive and effective tools for the real-time detection of associated biomarkers for early diagnosis. This is particularly needed for the diagnosis of papillary thyroid cancer, whose incidence has dramatically increased over the past few years in the United States and is predicted to increase in the next years, recording a greater frequency in the female population (Weir et al., 2015). Papillary thyroid cancer is the most common malignancy of the thyroid. Although it has favorable long-term survival in most cases, an early stage diagnosis is fundamental to start therapies that reduce mortality and lessen the associated endocrine disorders. The frequency of lymph nodes involvement is 27–46% at initial diagnosis and the recurrence rate is 3–30% during post-operative follow-up. Distinguishing lymph nodes metastasis from benign reactive lymphadenitis is therefore critical to rank the malignancy risks in patients with papillary thyroid cancer (Moon et al., 2013). Thyroglobulin (Tg) is a 660 kDa dimeric protein produced by and used entirely within the thyroid gland to produce the thyroid hormones thyroxine and triiodothyronine. Serum Tg levels are elevated in patients with goiter and in several other clinical conditions, and to date, the measurement of Tg is the mainstay in the post-surgical follow-up of differentiated thyroid cancer (Pacini and Pinchera, 1999). As thyroid-specific protein, its levels in lymph nodes are normally very low and an increased Tg level in the needle washout has been associated with metastasis of lymph nodes in patients affected by differentiated thyroid carcinoma (Giovanella et al., 2013). Its determination is currently based

* Corresponding authors.
*E-mail addresses:* menotti.ruvo@unina.it (M. Ruvo), anna.borriello@cnr.it (A. Borriello), a.cusano@unisannio.it (A. Cusano).
[1] These authors contributed equally to this work.

http://dx.doi.org/10.1016/j.bios.2016.02.021
0956-5663/

on immunometric-chemiluminescent or radioimmunometric assays (Spencer and Lopresti, 2008). The first methods require the use of enzyme-labeled monoclonal and polyclonal anti-Tg antibodies, assessing the presence of Tg by antibody-conjugated enzyme activity. Radioimmunometric assays are also based on the use of anti-Tg antibodies bearing specific radiolabels. Such techniques have lengthy incubation and washing steps, resulting excessively time-consuming. Moreover the need of labeled antibodies is a significant weakness, not allowing the real time detection of the target biomolecule and making conventional immunoassays techniques for Tg detection not easily amenable to clinical use. New effective, accurate, sensitive and rapid biosensing techniques are urgently needed.

In recent years efforts to define and optimize diagnostic and biosensing tools that incorporate such features are significantly increased. Molecular biosensors are preferred as clinical diagnostic tools than other traditional methods because of real-time measurement, rapid diagnosis, multi-target analyses, automation, and reduced costs. A few works have so far been proposed regarding Tg detection using a biosensor platform. In 2008 Choi et al. detected Tg in a cocktailed mixture of proteins by using the competitive protein adsorption/exchange reactions, namely Vroman effect. Implemented on a microfluidic system, the target protein displaced a pre-adsorbed weak-affinity protein on one surface of the device, while another pre-adsorbed high-affinity protein on an adjacent surface was not displaced. Differential measurement using surface plasmon resonance (SPR) phenomenon allowed Tg detection (Choi and Chae, 2009).

Recently Dantham et al. (2013) reported the detection of single human Tg protein molecule from the resonance frequency shift of a whispering gallery mode–nanoshell hybrid resonator upon adsorption on the nanoshell. However, although the high sensitivity of the proposed devices, the absence of a bioreceptor featuring high specificity and affinity, which can then discriminate between target and non-target molecules, prevented the use of such systems in clinical and diagnostic applications.

Moreover in the last years, the continuous demand for lower limits of detection combined with cost effectiveness and reliability features has been the driving force for the successful demonstration of optical label free biosensors with impressive figures of merit (Fan et al., 2008; Hoa et al., 2007). Relative principles of operation include SPR (Chung et al., 2006; Teramura and Iwata, 2007), interferometry (Weisser et al., 1999; Schneider et al., 1997), optical waveguide-based biosensors (Website, http://www.neosensors.com), optical ring resonators (Chao et al., 2006; Ren et al., 2007; Hanumegowda et al., 2005), fiber-based biosensors (Lee and Fauchet, 2007; Skivesen et al., 2007, Chryssis et al., 2005; DeLisa et al., 2000; Zhang et al., 2005). Among the others, fiber optic optrodes constitute a valuable platform for label biosensing because of its intrinsic biocompatibility, compact size, multiplexing capability, remote operation and easy integration in medical needles. In particular, in this work we selected optical fiber LPGs as evanescent wave-based biosensors for the measurements of local refractive changes due to molecular binding occurring at the sensor surface (Pilla et al., 2011; 2012a, 2009; Del Villar et al., 2005; Cusano et al., 2006).

An LPG consists of a periodic modulation of the RI at the core of an optical fiber that results in the coupling of the light between core and cladding modes (James and Tatam, 2003). Thanks to the huge sensitivity to surrounding refractive index (SRI) changes, LPGs represent a very promising technological platform, which can be employed in a wide number of chemical and biological applications (Chiavaioli et al., 2014; Eftimov, 2010; Baldini et al., 2012; Tripathi et al., 2012; Smietana et al., 2015; Falciai et al., 2001; Falate et al., 2005; Chen et al., 2007; Ramachandran et al., 2002). The main disadvantage of LPG biosensors experienced so far is the intrinsic transmission mode operation, which makes the optical device sensitive to bending, difficult to use in *in vitro* assays and, more importantly, creates a significant barrier for their integration in hypodermic needles. Hence, a reflection-type configuration would be desirable to combine the high sensitivity featured by this kind of devices with the unrivaled advantages of single ended optrode configurations (Garg et al., 2013; Huang et al., 2013; Consales et al., 2014; Alwis et al., 2013; Cao et al., 2013).

On this line, we present in this work the development of a reflection-type LPG biosensor able to perform the detection of thyroid cancer biomarkers in the needle washouts of fine-needle aspiration biopsies. After fabrication, the reflection-type LPG is functionalized with a hydrophobic coating of a specific bioreceptor, in our case an anti-Tg monoclonal antibody and the protein is detected in label-free experiments. Results clearly demonstrate the effectiveness and sensibility of the biosensing platform, allowing the *in vitro* detection of sub ng/ml concentrations of human purified Tg. To validate the potential translation of such LPG-based biosensor into the clinical practice, detection experiments on clinical samples have been carried out.

## 2. Materials and methods

### 2.1. Chemicals

Ethanol (EtOH), isopropyl alcohol (IPA, analytical grade 99.7), double distilled water ($ddH_2O$), chloroform ($CHCl_3$, analytical grade 99.9), atactic polystyrene (aPS, MW=280.000 g/mol), aqueous ammonia ($NH_3$ 30% w/w), dextrose, human Thyroglobulin (T6830-5MG), 4-(2-hydroxyethyl)-1-piperazineethanesulfonic acid (10 mM), 1% bovine serum albumin (BSA) solution and HRP conjugated-streptavidin (GERPN1231-100UL), chromogenic substrate, 3,3′,5,5′-Tetramethylbenzidine (TMB) were purchased from Sigma-Aldrich (Milan, Italy). Anti-Tg mouse monoclonal antibody (Ab, MA5-12048) was purchased from Thermo Scientific (Monza, Italy). Potassium hydroxide solution (KOH) was purchased by J.T. Baker.

### 2.2. Reflection type LPGs (RT-LPG) design, fabrication and characterization

The LPGs used in this experiment were UV-written in boron doped photosensitive single-mode optical fibers (PS1250/1500, Fibercore Ltd.) using a point-to-point technique. LPGs were coated with a nano-scale high refractive index (HRI) layer of aPS in order to tune the working point of the device in the modal transition region, allowing to attain giant SRI sensitivities (of the order of thousands of nm/RIU) (Del Villar et al., 2005; Cusano et al., 2006), and at the same time provide a suitable surface for the hydrophobic adsorption of the bioreceptor.

#### 2.2.1. LPG inscription

For the LPG inscription, the fiber was mounted on an automatic rotation stage able to continuously rotate the optical fiber during the writing grating procedure with a KrF pulsed excimer laser (LightBenth 1000, Optec, Belgium) operating at a wavelength of 248 nm. Moreover, both the rotation stage and the laser action were controlled and synchronized by a personal computer in order to select the grating pitch (translation stage step and slit dimension), the grating length (number of irradiated points) and the induced RI change (number of laser pulses per point and fluence).

#### 2.2.2. Design of transition mode HRI-coated LPG

The matrix method with the Linearly Polarized (LP) mode approximation (Del Villar et al., 2005; Pilla et al., 2012b) was used to

identify the optimal design parameters of the transition-mode HRI-coated LPG biosensors, including the grating period, the cladding mode order and the aPS overlay thickness. The parameters of the optical fiber used for the simulations are contained in the specifications of the Fiber-core PS1250/1500: core and cladding radii of 3.5 μm and 63 μm, respectively and numerical aperture of 0.13. One of the most useful and practical tools for the LPGs design is the modal dispersion plot (MDP), which allows to recognize which modes (and at which wavelengths) are excited depending on the chosen grating period ($\Lambda$). The MDP has been used to identify the optimal pair LPG period-aPS thickness that optimize the sensitivity of the final device, with the constrain of keeping the operating wavelength in a range around 1550 nm in order to work in the optical telecommunication windows and benefit of low cost optoelectronic equipments.

#### 2.2.3. RT-LPG transducer fabrication

On the basis of the theoretical results (reported in Section 3.1), a customized LPG ($\Lambda = 370$ μm) written in a photosensitive standard single-mode fiber (Fibercore PS1250/1500) was used for the biosensor fabrication. The main steps to realize the RT-LPG transducer relies on (i) the fiber cutting just at the end of the grating, (ii) the integration of a completely reflecting layer (*i.e.* an Ag mirror) on the fiber end-face and (iii) the aPS overlay deposition on the RT-LPG surface. The first step (i) is of fundamental importance for the development of a more practical and robust LPG working in reflection configuration, and was dictated by our biomedical applications, which required the probe to be immersed into laboratory vials containing the biological samples under tests. A crucial aspect in this step is the identification of the precise grating location along the optical fiber, in order to cut it just after the grating end in order to avoid the formation of interference fringes within the attenuation bands, typical of self-interfering LPGs (Alwis et al., 2013). Once identified the LPG, the fiber was cut just after the grating by using a high precision cleaver (Fujikura CT-30).

Successively, for the silver mirror integration on the tip of the optical fiber, a freshly prepared silver nitrate solution ($AgNO_3$ 0.1 M, 640 μL) and a potassium hydroxide solution (KOH 0.8 M, 440 μL) were mixed. The brown precipitate formed was dissolved by addition of aqueous ammonia ($NH_3$ 30% w/w, 2 drops) with stirring and a dextrose solution (0.25 M, 64 μL) was added. After stirring, the LPG tip was dipped into the ready Tollen's reagent (Yin et al., 2002). The fiber was removed after ~30 min (though the silver film formed on the wall of vial in 5 min) and air-dried.

Finally, the RT-LPG was coated with a thin layer of aPS by means of the dip-coating (DC) technique. In particular, the DC was performed by means of an automated system (NIMA Technology Micro-Processor Interface IU 4) at an immersion/extraction speed of 100 mm/min. Deposition solution was: 9.5% (w/w) of atactic polystyrene (aPS) in chloroform.

#### 2.2.4. RT-LPG transducer characterization, interrogation setup and data analysis

The spectral characterization of the fabricated LPG *versus* SRI has been carried out by submerging the probe into aqueous glycerol solutions characterized by different RI in the range 1.335–1.460, in order to validate the fabrication process success and the SRI sensitivity in correspondence of an SRI = 1.34. To this aim, an optoelectronic set-up comprising a broadband light source (with bandwidth 1200–1700 nm), a $2 \times 1$ directional coupler and an optical spectrum analyzer (OSA, ANDO AQ6317C, wavelength resolution 10 pm, dynamic range 60 dB) was used for the acquisition of the LPG reflection spectrum at the different stages of the device fabrication and characterization. The OSA is connected to a personal computer and controlled by a LabView plug-in, enabling the automatic acquisition of the RT-LPG spectra. Acquired spectra are then automatically filtered and elaborated by a MATLAB script that provides the central resonance wavelengths ($\lambda c$) of each spectrum. During the biological experiments the RT-LPG spectra is automatically acquired every 45 s, thus providing a continuous and real time monitoring of the interaction kinetics of the biological molecules on the RT-LPG surface.

### 2.3. Bioreceptor selection, characterization and affinity study

#### 2.3.1. Thyroglobulin ligand selection and characterization

Several monoclonal antibodies against Tg are commercially available. Among the others, anti-Thyroglobulin Mouse Monoclonal Antibody MA5-12048 from Pierce Thermo Scientific has been used in several applications (Ko et al., 2012; Magro et al., 2003; Endo and Kobayashi, 2011). We therefore choose such reagent for the detection of Tg in biochemical assays. Before use, the mAb underwent several biochemical characterization including ELISA and SPR binding to Tg to estimate the dissociation constant ($K_D$) and antigen specificity.

#### 2.3.2. Ligand characterization by ELISA assays

The binding between Tg and the mAb was firstly monitored by ELISA. Assays were performed adsorbing human Tg on 96-microwell plates (MaxiSorp™, Nunc, Milan, Italy). Wells were filled with 100 μL PBS buffer (10 mM $Na_2HPO_4$, 2 mM $KH_2PO_4$, 137 mM NaCl, 2.7 mM KCl, pH 7.4) containing Tg at 1.0 μg/mL for 16 h at 4 °C. After coating, plates were washed with PBS-T buffer (PBS containing 0.005% Tween-20), then 300 μL blocking solution containing 1% BSA in PBS were added and incubated for 1 h at 37 °C. After washing again with PBS-T solution, 100 μL solutions containing increasing concentrations of anti-Tg mouse monoclonal antibody were added and incubated for 1 h at 37 °C. Following washing, 100 μL of HRP-conjugated Goat anti-mouse IgG antibody diluted 1:1000 were added and incubated for 1 h at 37 °C. Finally plates were washed with PBS-T solution and detection was achieved by adding 100 μL of chromogenic substrate, 3,3′,5,5′-Tetramethylbenzidine (TMB). The reaction was stopped by addition of 50 μL of 2 M $H_2SO_4$ after 10 min. Absorbance was measured at 450 nm with an EnSpire multimode plate reader (Perkin Elmer, Waltham, Massachusetts). Data were fitted using GraphPad Prism 4 software (GraphPad Software, San Diego, California).

#### 2.3.3. Ligand characterization by label-free SPR assays

Tg binding to mAb and the $K_D$ estimated by ELISA were further confirmed by SPR real time binding assays performed on a Biacore 3000 Instrument (GE Healthcare). The amino coupling kit and CM5 sensor chips were from Biacore GE Healthcare. Surface preparation and binding assays were carried out in HBS-EP buffer (10 mM HEPES, 150 mM NaCl, 3 mM EDTA, pH 7.4, Surfactant P-20 0.005%). The COOH surface was activated injecting 100 μL of EDC [0.4 M]/NHS [0.1 M] (1:1 M ratio) solution at a flow rate of 10 μL/min. Binding was performed by immobilizing both the mAb and Tg on distinct channels. For Tg immobilization, the protein at 5.0 μg/mL in acetate buffer pH 4.5 was injected after EDC/NHS activation over the chip at a flow rate of 10 μL/min for a total contact time of 10 min. For mAb immobilization, it was similarly used at 5.0 μg/mL in acetate buffer pH 4.5. Residual reactive groups were deactivated by treatment with 50 μL of 1 M ethanolamine hydrochloride, pH 8.5 at a flow rate of 10 μL/min. Blank channels were prepared by performing the same immobilization steps without proteins. Binding assays were performed by injecting human Tg at increasing concentrations in HBS-EP over the mAb-derivatized chip at a flow rate of 10 μL/min. Binding of soluble mAb to immobilized Tg was carried out under similar conditions injecting the antibody at increasing concentrations in HBS-

EP at a flow rate of 10 μL/min. In both experiments, the baseline was restored using 10 μL pulses of 5 mM NaOH. Data were manipulated to obtain kinetic and thermodynamic parameters using BIAevaluation software. Data fitting was carried out using 1:1 binding models. Non-specific binding from blank channels was subtracted prior to analysis. $K_D$s for any single binding experiment were obtained as ratio between $K_{off}$ and $K_{on}$. Final $K_D$s were obtained by averaging the values from experiments at the different concentrations.

### 2.4. Quantitative Thyroglobulin detection with LPGs

#### 2.4.1. In vitro dose–response assay and Tg calibration curve on LPG biosensors

A dose-dependent assay was performed to obtain a calibration curve for the semi-quantitative detection of human Tg using RT-LPG biosensors. Several different biosensors were prepared to probe Tg solutions at increasing concentrations. For any distinct biosensor, the selected anti-Tg mAb was hydrophobically adsorbed on the optical fiber active surface by immersing the fiber tip in a solution of mAb at 15 μg/mL for 2 h at room temperature. This antibody concentration was chosen after several tests whereby detectable Tg was evaluated as a function of antibody immobilization. Probes were then washed with fresh buffer and immersed in 1% BSA solution in 10 mM HEPES buffer, pH 7.0 for 1 h. The different LPG biosensors were dipped into 1.0 mL samples of human Tg solution at 0.08 ng/mL, 0.80 ng/mL, 4.0 ng/mL, 8.0 ng/mL, 40 ng/mL and 80 ng/mL (corresponding to 0.12 pM, 1.2 pM, 6.0 pM, 12.1 pM, 60.1, 121.0 pM, respectively) and the observed resonance wavelength shifts recorded. Although the fabrication process was robust and repeatable, a normalization procedure was needed to account for the even tiny differences of device performances. Such differences may occur due to the LPG fabrication tolerances, or to slightly different antibody coatings obtained on the distinct devices. To normalize the signals we used the wavelength shift occurred upon mAb coating, as an indirect measure of surface sensitivity of each LPG probe. We thus calculated the final observable ($O$) as reported in the following Eq. (I):

$$\text{Observable } (O) = \frac{\Delta\lambda_{Tg-binding}}{\Delta\lambda_{mAb-coating}} \quad \text{(I)}$$

where, $\Delta\lambda_{Tg\text{-}binding}$ and $\Delta\lambda_{mAb\text{-}coating}$ are the differences between the stabilized central wavelength of the attenuation band in buffer solutions before and after contact with the biomolecule solution and denote Tg binding and mAb coating onto the LPG surface, respectively. Data were fitted using SigmaPlot 10.0 software. Data fitting was carried out using 1:1 model. The $K_D$ was determined by reporting the observed resonance peak shift at every concentration *versus* analyte concentration. Some antibody-coated optical fibers were immersed in buffer alone and used as blank.

#### 2.4.2. Assessing Tg capture on the LPG biosensors surface by on-fiber ELISA-like assays

To assess the specific capture of Tg on the surface of the RT-LPG biosensor surface, we set-up and performed a parallel assay whereby Tg binding to the adsorbed antibody was monitored by both LPG and by an ELISA-like assay. Assays were performed adsorbing the anti-Tg mAb on the surface of an LPG biosensor as described in the previous section (named "LPG" biosensor). The same protocol was used, in parallel, on a fiber without LPG inscription to perform the ELISA-like assay (named "control+" biosensor). On the RT-LPG biosensor, output signal variations were monitored in real time. A third fiber without antibody coating was used as negative control (named "control−" biosensor). After coating, all optical fibers were thoroughly washed with buffer and subsequently dipped in 1% BSA solutions in the same HEPES buffer (BSA, Sigma-Aldrich) for 1 h at room temperature. After washing again the optical fibers with plenty of fresh buffer, they were immersed in 1 mL of biotinylated human Tg solution at 40 μg/mL (60.1 nM) and incubated for 1 h at room temperature. Biotinylation was required for Tg detection using the streptavidin-HRP system. Following washing, all biosensors were dipped into 1 mL of HRP conjugated-streptavidin 1:5000 dilution in 10 mL HEPES pH 7.0 for 1 h at room temperature. Finally, all optical fibers were washed again and detection was achieved by immersing the probes in 300 μL of Quantared Enhanced Chemifluorescent HRP substrate (Thermo Scientific), for 10 min at room temperature. Relative fluorescence released from the fiber surface was determined using an EnSpire multimode plate reader (Perkin Elmer, Waltham, Massachusetts) after transferring the solutions into a 96-well plate. Excitation and emission maxima used were 570 nm and 585 nm, respectively. The same binding experiment with biotinylated Tg was firstly performed on microtiter ELISA plates to assess the binding and to set up the experimental conditions (not shown).

Tg was biotinylated using Biotin N-hydroxysuccinimide ester (Biotin–NHS, Sigma Aldrich) as reported elsewhere for other proteins (Tornatore et al., 2008). Briefly, to 300 μg protein in 500 μL PBS (final concentration 909 nM), 0.7 μL of 10 mM Biotin–NHS solution in DMSO were added and the mix left in ice for 30 min. Then 250 μL Tris 50 mM pH 8.0 were added to stop the reaction and the biotinylated protein was finally micro-dialyzed against PBS to remove the excess biotin and glycine. Stock solution of protein at 0.30 mg/mL (454 nM) were prepared and stored frozen at −80 °C.

### 2.5. Clinical sample preparation

Several needle washouts of thyroid tissue or suspected lymph nodes have been prepared. After the approval of the Ethical committee at University of Napoli Federico II (790/2014), syringes used for fine needle biopsies for classical cytology have been washed in 1 ml of PBS solution. Samples have been split in two, and one half was stored at −80 °C until usage, while Tg concentration has been measured in the second half of the sample using the Immulite 2000 Tg kit (Siemens Healthcare Diagnostic Products, UK) with a nominal sensitivity of 0.9 ng/mL (1.4 pM).

### 2.6. Determining Tg on clinical samples

LPG biosensors were used to *ex-vivo* detect human Tg from the needle washout of fine-needle aspiration biopsy. After a biochemical functionalization of the LPG sensitive area with the anti-Tg monoclonal antibody, probes were immersed in the saline diluted needle washouts of fine-needle aspiration biopsies from several patients containing different human Tg amounts and the observed resonance wavelength shifts were recorded. In such samples, Tg was previously quantified by canonical techniques as described in the previous section. Data were normalized following formula (I) and subsequently fitted using SigmaPlot 10.0 software. Data fitting was carried out using a 1:1 model. The $K_D$ was determined by reporting the observed resonance peak shift at different concentration *versus* analyte concentration.

## 3. Results and discussions

### 3.1. Nano-scale HRI coated-LPG design

In Fig. 1a, the MDP for some high-order cladding modes ($LP_{05}$–$LP_{07}$) is shown. In particular, SRI was set to 1 for the bare LPG (bold

curve), while it was set to 1.34 for the dashed green curves (referred to the mode $LP_{07}$ in the aPS-coated device) (aPS RI = 1.555), to achieve the optimal design parameters in correspondence of the RI of phosphate buffer solution used in our detection experiments. In Fig. 1a, the red horizontal line shows the operating wavelength of 1550 nm. When the effective RI of the cladding modes increases due to either an SRI increase, an HRI overlay deposition or to a combination of the two, the modal curves move towards the position originally occupied by the curve of the nearest lower mode before the perturbation. In line of principle, the maximum sensitivity is obtained at the center of the transition of a mode towards the previous one (Pilla et al., 2012b): on the basis of this observation, it is possible to choose the pair period. In particular, by choosing a period of 370 μm (red vertical line) and an aPS overlay thickness ($t_{aPS}$) of 310 nm, the curve related to the $LP_{07}$ mode for a SRI = 1.34 is approximately in the maximum of the modal transition. This is more evident in Fig. 1b which shows the relationship between the grating period $\Lambda$ and the overlay thickness $t_{aPS}$ for some order cladding modes ($LP_{05}$, $LP_{06}$, and $LP_{07}$), fixing the wavelength at 1550 nm and the external refractive index (RI) to 1.34. The sensitivity to SRI changes is also shown in modulus on a color bar. The rectangle shows the modal transition zone. From Fig. 1b it can be noted that the $LP_{07}$ mode exhibits the maximum sensitivity (about 1690 nm/RIU) in correspondence of the pair period $\Lambda = 370$ μm and thickness $t_{aPS} = 310$ nm. The maximum sensitivity also increases with the mode order thus suggesting designing gratings with shorter periods (*i.e.* higher order modes, e.g. $LP_{08}$, $LP_{09}$…). However, it is worth noting that sometimes it is preferable to work with lower mode orders to reduce instabilities and facilitate the device handling, both in the fabrication and testing stage.

### 3.2. Fabrication and characterization of the RT-LPG

Fig. 2a reports the transmission spectrum of the attenuation band associated to the sixth order mode cladding acquired before the optical fiber cut (blue line), the reflected spectra after the optical fiber cut (red line), and after the silver layer formation at the fiber facet (green line).

As shown in Fig. 2a, a significant baseline reduction of 15 dB occurs after the cut, mainly due to the fact that light passing through the LPG is mostly transmitted at the fiber/air interface, and only a small portion of it is reflected back into the fiber. Nevertheless, after the Ag mirror layer formation at the fiber end face, almost all the initial power is recovered. We point out that the use of reflection-type LPGs not only is of fundamental importance to transform an LPG-based sensor in a more practical probe for concrete biomedical applications, but also enables to improve the resonance visibility (see Fig. 2a) due to the double passing of light through the grating. The last fabrication step relied on the aPS overlay deposition onto the RT-LPG surface using the DC technique, as reported in Section 2. Fig. 2b reports the spectral position of the sixth order cladding mode in the bare RT-LPG (blue curve) and after the aPS overlay deposition (red curve). All the spectra were recorded with the device surrounded by air.

The deposition of a HRI layer overlay onto the grating increases the effective RI of the cladding modes and, as a consequence, the attenuation bands undergo a blue shift, which for the sixth order cladding mode is about 27 nm after the aPS layer deposition. In particular, the resulting overlay thickness after DC from the 9.5% PS solution was ~310 nm, as retrieved by means of a reverse engineering approach carried out with the help of numerical simulations of nano-scale coated LPGs.

The spectral characterization of the fabricated LPG *versus* SRI has been carried out by submerging the probe into aqueous glycerol solutions characterized by different RI in the range 1.335–1.460. The obtained SRI sensitivity ($|\partial\lambda_c/\partial SRI|$) exhibits the typical resonance-shaped behavior of transition mode LPG, thus confirming the fabrication process success. At the same time, it can be seen that the SRI sensitivity in correspondence of an SRI = 1.34 is equals to ~1700 nm/RIU. This experimental value resulted slightly higher than those obtained from the design process (~1690 nm/RIU), probably due to the slight differences between numerical and experimental values of aPS layer and glycerol solutions RIs (used for SRI sensitivity characteristic and measured at 589 nm and for which dispersion was not taken into consideration).

### 3.3. Characterization of the Tg/anti-Tg mAb interaction

#### 3.3.1. ELISA characterization

Thyroglobulin is a 660 kDa dimeric protein produced by the thyroid gland to generate the thyroid hormones thyroxine and triiodothyronine. Serum Tg levels are elevated in patients with goiter and high Tg levels can be detected in the needle washout of metastatic lymph nodes in patients with differentiated thyroid carcinoma (Giovanella et al., 2013). Tg is mostly detected and quantified in biological fluids by ELISA using monoclonal antibodies (mAbs), which are very sensitive and specific reagents. mAbs are also highly resistant to denaturation and degradation compared to other proteins given the intrinsic globular, high β-sheet containing structure. As a Tg bioreceptor we choose one of the several commercially available anti-Tg monoclonal antibodies because such reagents are generally characterized by extremely

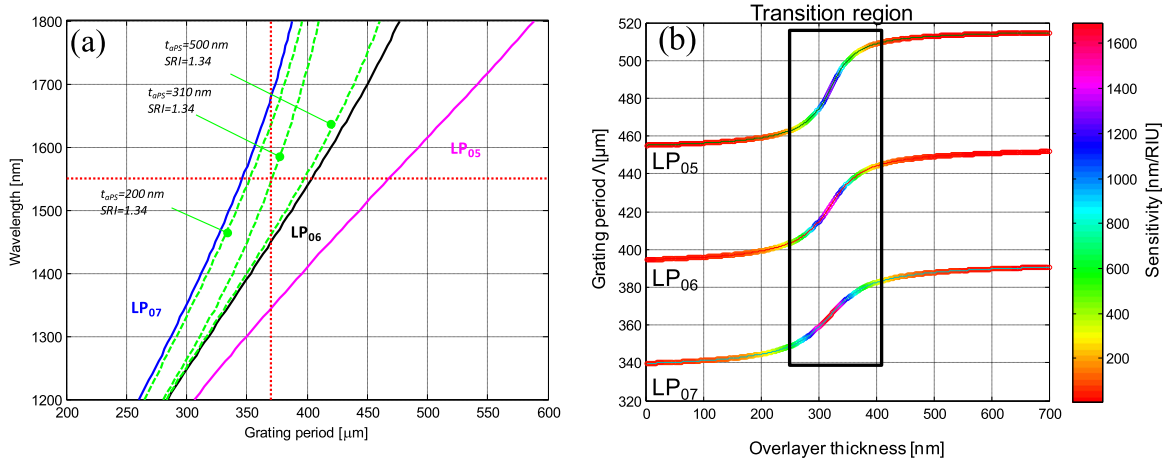


**Fig. 1.** (a) Modal dispersion diagram: $LP_{07}$, (b) Grating period *versus* aPS overlay thickness for the $LP_{05}$, $LP_{06}$ and $LP_{07}$, the SRI sensitivity of each mode is also reported in the color bar. (For interpretation of the references to color in this figure legend, the reader is referred to the web version of this article.)

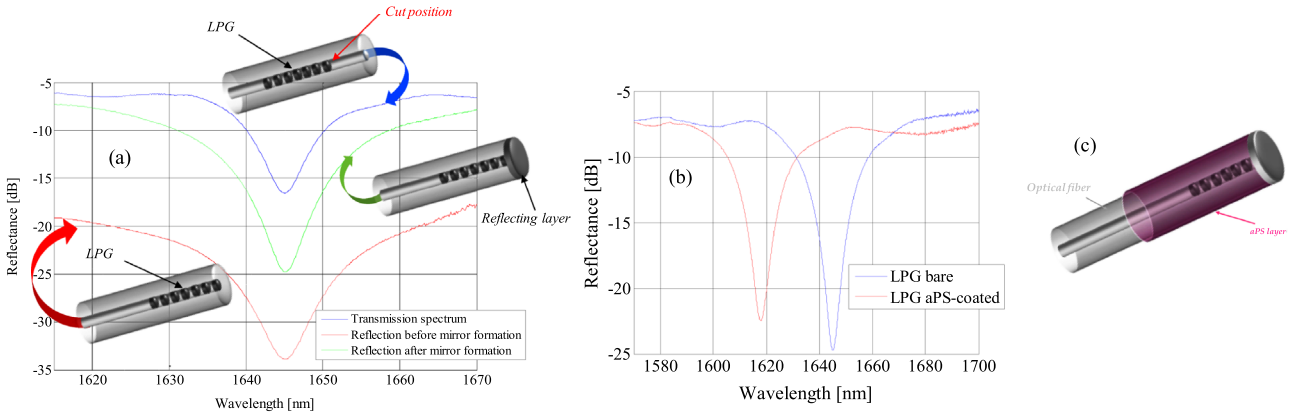


**Fig. 2.** (a) LPG spectra acquired in air before the fiber cut (blue curve), just after the fiber cut (red curve) and after the mirror integration (green curve) and schematics of the reflection-type LPG fabrication steps (in the insets), (b) spectra of the bare (blue line) and aPS-coated (red line) RT-LPG, (c) Schematic of the final RT-LPG prototype. (For interpretation of the references to color in this figure legend, the reader is referred to the web version of this article.)

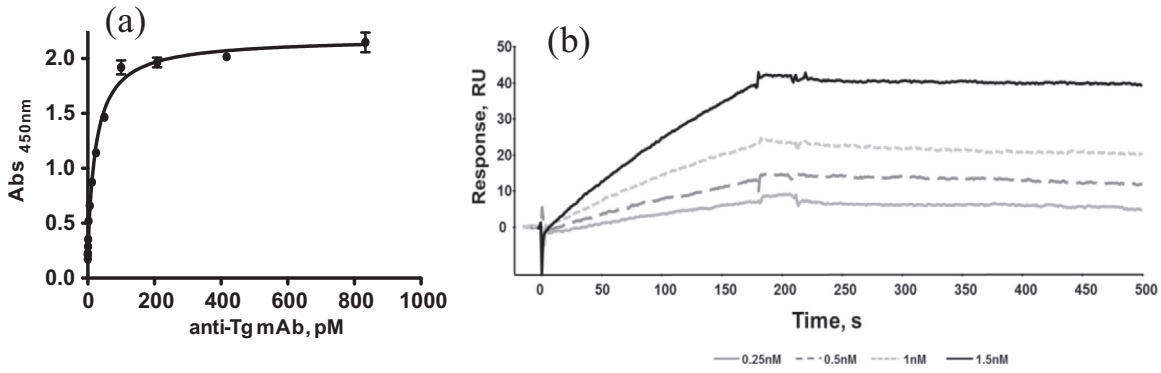


**Fig. 3.** Biochemical system characterization. (a) Dose–response indirect ELISA assay performed to assess antigen/antibody affinity. (b) SPR assay using Biacore of the binding kinetic of anti-Tg monoclonal antibody to immobilized Tg, at different antibody concentrations.

high specificity and affinity for the target molecules. The anti-Tg antibody has been already described in the literature and is sufficiently specific to detect Tg also in immunohistochemistry experimental settings (Ko et al., 2012; Magro et al., 2003; Endo and Kobayashi, 2011). The affinity of the monoclonal antibody for Tg was assessed using both traditional immunoenzymatic and real-time assays. An indirect ELISA was firstly performed by adsorbing Tg on multiwell plates and adding increasing amounts of the mouse anti-Tg monoclonal antibody (Fig. 3a). Following the detection step with an anti-mouse antibody conjugated with HRP, increasing chromogenic signals (corresponding to increased bound analyte) were recorded with increasing antibody concentration. As shown in Fig. 3a, a strong and saturable binding signal was observed even at low antibody concentrations. Saturation started at 100 pM mAb (66 ng/mL). Fitting of data points by a non-linear algorithm, where we assumed a 1:1 binding stoichiometry, provided a $K_D$ of 72 pM, a value indicative of the high affinity of the antibody for the specific analyte. The presence of high concentrations of BSA in the assay (1% w/w, that is 10 mg/mL), further provided an indication of selectivity. Indeed blank signals were negligible and after subtraction a 2.0 AU residual signal was measured at saturation.

### 3.3.2. SPR characterization

To further characterize the binding between the antibody and Tg, we next performed a label free binding assay using an SPR-based instrument (BIAcore). The anti-Tg antibody and Tg were thereby immobilized on the surface of the sensor chip (1120 and 650 RU immobilization level, respectively. Not shown). In one experiment with the Tg-derivatized chip, mAb solutions at increasing concentrations, between 0.25 and 1.5 nM (165 ng/mL and 990 ng/mL), were injected. As shown in Fig. 3b, dose–response association and dissociation curves were obtained witnessing the high affinity and specificity of the interaction. Using the kinetic parameters a $K_D$ of 70 pM was estimated. This value was in full agreement with that extrapolated by ELISA, confirming the strength of the interaction and the high specificity. When we probed the immobilized antibody with soluble Tg a significantly higher $K_D$ (about 1.3 nM) was determined (data not shown) than that determined by ELISA. This was likely due to inappropriate antibody immobilization.

### 3.4. Assessment of Tg capture on LPG biosensor surface by on-fiber ELISA-like assay

A major step to validate a prototype biosensor for cancer biomarker detection is to demonstrate its capability to capture the wished analyte. One critical point is the assessment of the binding event observed with a prototype platform, as in the present case, with a well-established and alternative approach. Immunoenzymatic and label-free techniques are typically used to independently assess the experimental setting and to characterize and monitor the interactions involved in the experiments (Pilla et al., 2012a; Brzozowska et al., 2015). However, to the best of our knowledge, no reports have so far described the use of alternative approaches for the parallel measurement of the analyte captured on the surface of the prototype biosensor. To this aim, we developed an on-fiber ELISA-like assay (see cartoon in Fig. 4a) to monitor in parallel the binding event observed in real time with the resonance wavelength shift.

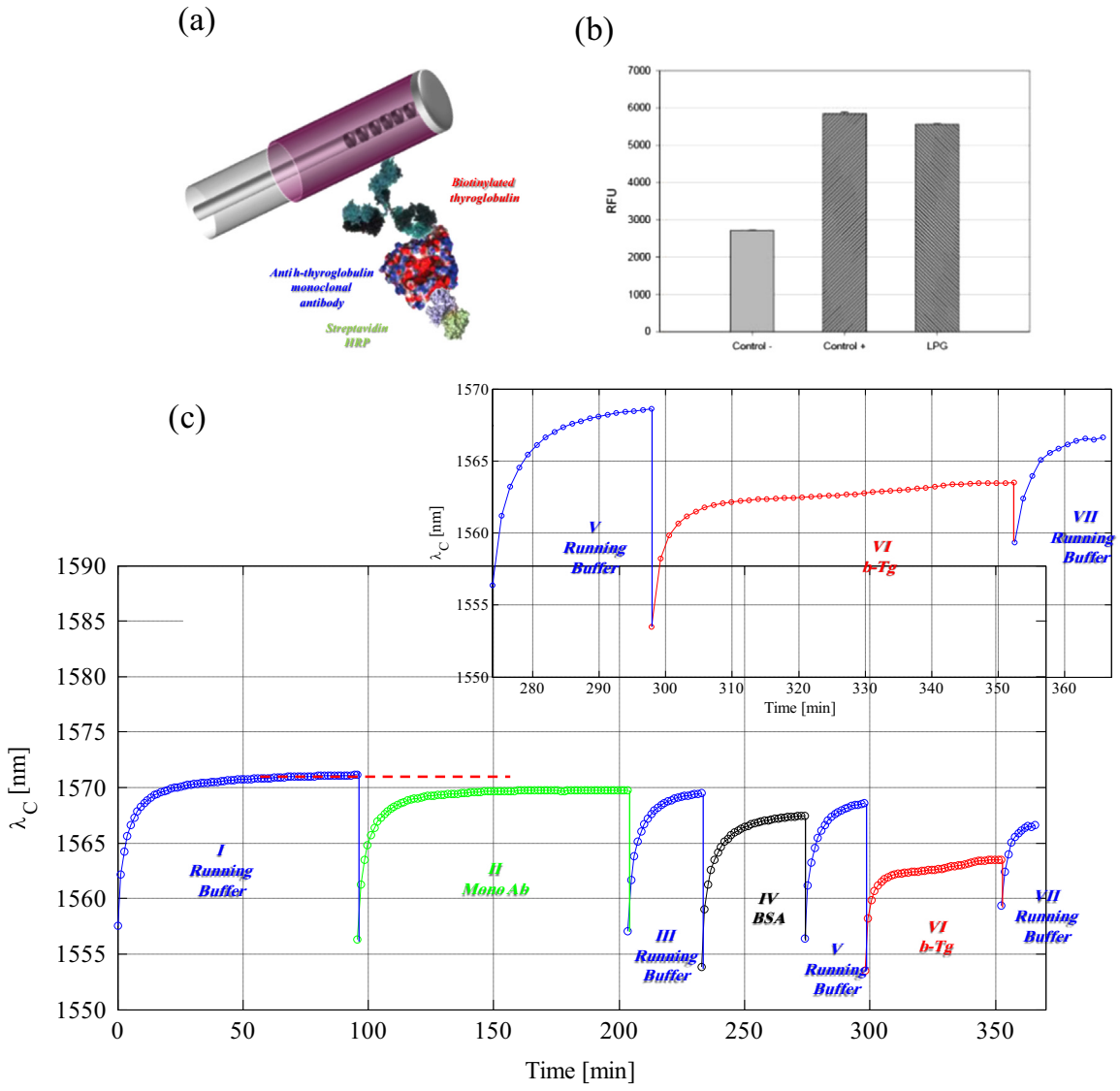


**Fig. 4.** On-fiber ELISA-like assay and biotinylated Tg detection. (a) schematic view of the on-fiber ELISA-like assay. (b) Binding signals obtained by the ELISA-like assay. "Control−" is an optical fiber without monoclonal antibody coating, "LPG" is a RT-LPG probe used for the ELISA-like confirmation assay. (c) RT-LPG sensorgram reporting the wavelength shift of 6th order cladding mode attenuation band during 40 μg/mL (60.6 nM) biotinylated Thyroglobulin detection assay. In magnification the wavelength shift during binding event is reported.

The experiment was thus performed in parallel on three distinct fibers, the "LPG", the "control+" and the "control−", as described in Section 2. Following antibody adsorption on the "LPG" and "control+" probes *via* hydrophobic coating, we performed all steps required for the ELISA-like assay (BSA blocking, biotinylated-Tg capture and HRP-conjugated streptavidin addition) on all fibers including the "control−" one (see cartoon in Fig. 4a). On the RT-LPG biosensor the resonance wavelength variations in real time were also monitored. In Fig. 4b results obtained from the ELISA-like assay are reported, expressed as Relative Fluorescence Units (RFU). Both the "LPG" and "control+" fibers with the coated antibody provided fluorescence signals of 5773 and 5627 RFU, without statistically significant differences between them, whereas the negative control, where no antibody was coated, showed a significantly lower fluorescence emission of 2715 RFU. It must be underlined that signals observed for the RT-LPG transducer and the positive control were approximately twice the signal observed for the negative control. The signal detected on the negative control fiber was most likely due to non-specific adsorption of biotinylated Tg and conjugated streptavidin on the optical fiber surface. Data obtained with the on-fiber ELISA-like assay are suggestive of a specific binding of biotinylated Tg to the antibody on both "control+" and "LPG" fibers, since much less bound analyte was detected on antibody uncoated fibers. Dynamics of biomolecular binding were also monitored in real time on the LPG fiber with the optoelectronic setup described in Section 2.5 and Fig. 4c shows a typical sensorgram obtained for the binding of biotinylated Tg to immobilized antibody. The measured resonance wavelength ($\lambda_c$) is reported as a function of time. During the analyses, we observed several relevant steps, from I to VII. At the beginning, the coated RT-LPG was immersed for approximately 90 min in a vial containing HEPES buffer until signal stabilization (step I). A huge resonance wavelength red shift from 1557 nm to 1571 nm was recorded during this step. Subsequently, the optical fiber was dislodged from the solution and immediately immersed in a vial containing the anti-Tg monoclonal antibody solution for 2 h (step II). This time interval was required for the physical adsorption of the mAb on the aPS surface; we measured a 2.0 nm resonance peak shift due to the contribution of the bulk RI solution and the formation, on the probe surface, of the antibody layer,

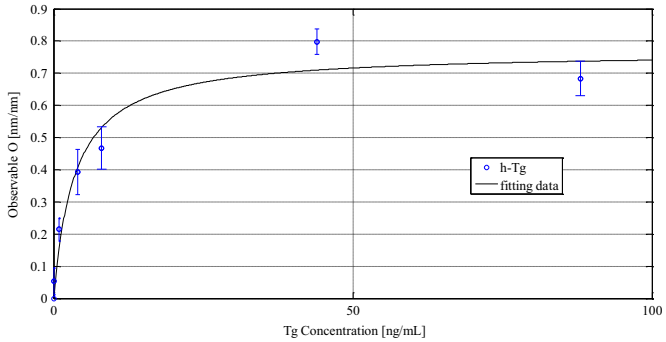


**Fig. 5.** Calibration curve for the semi-quantitative detection of human Thyroglobulin using RT-LPG biosensor. Blue dots refer to the dose-dependent assay performed to obtain the calibration curve.

increasing the effective RI of the cladding modes. To avoid the influence of bulk RI change due to solutions with different compositions, and to estimate the net resonance peak shift due to the antibody coating formation, the probe was removed from the solution and, after fast and repeated immersions in the washing solution, the fiber was plunged again in HEPES buffer (step III). In this way peak shifts were estimated as a difference between two subsequent immersions in the HEPES buffer, specifically before and after dipping the sensor in the antibody solution. Inefficiently bound antibodies were completely removed in the washing step, therefore we assumed that the wavelength shift between plateau levels before antibody coating and after washing, was ascribed only to the stable layer of antibody on the LPG, with no influence of the differences of the bulk RI.

We thus evaluated the wavelength variation associated to the biomolecule layer formation considering the difference between the stabilized central wavelength of the attenuation band ($\Delta\lambda$) in buffer solutions before and after contact with the biomolecule solution. Since the measured refractive indices of the buffer solution before and after antibody deposition are identical, we inferred that the antibody not-permanently bound to the fiber surface was completely removed by the washing cycles. After signal stabilization, the RT-LPG resonance wavelength blue shift recorded between steps I and III ($\Delta\lambda_{\mathrm{I-III}}$) was 1.8 nm, indicating the formation of a stable antibody layer on the surface of the LPG transducer. The blocking step was finally performed by immersing the probe in a 1% solution of BSA for 1 h (step IV), recording a blue shift for the optical signal ($\Delta\lambda_{\mathrm{IV-V}}$) of 2.5 nm. This step was necessary to minimize non-specific protein adsorption and to cover potentially uncoated areas of the sensor surface. Again, to estimate the net contribution of BSA adsorption, depleted of the influence of bulk RI changes, the probe was removed from the solution, rapidly rinsed with washing solution and immersed in HEPES buffer (step V), observing a blue shift for the optical signal ($\Delta\lambda_{\mathrm{III-V}}$) of 0.8 nm between steps III and V. It must be noted that every time the grating was extracted and submerged into a new solution, a sort of acclimatization of the polymer layer was observed as a fast red wavelength shift, followed by a slow adaptation of the polymer. The probe, functionalized with the antibody, was immersed in a solution of biotinylated human Tg at 40 μg/mL (60.6 nM) and incubated for 1 h at room temperature to allow analyte capture and stabilization of the binding (step VI). During this step a huge blue shift of the resonance peak was observed. After analyte capture (see magnification in Fig. 4c), the probe was rinsed by fast immersions in washing solution and then moved into HEPES buffer, observing a blue shift of the resonant peak ($\Delta\lambda_{\mathrm{V-VII}}$) of 2.0 nm. Such shift was a measure of the effective binding between the anti-Tg monoclonal antibody and the biotinylated antigen.

### 3.5. Calibration curve for the detection of human Thyroglobulin with LPG biosensor

To use the platform for the detection of Tg in biological fluids, we first evaluated the system dose–response features and the associated sensitivity. The system was therefore tested on a set of several different Tg solutions at different concentrations ranging between 0.08 ng/mL (0.13 pM) to 88 ng/mL (133 pM). Since no regeneration steps were carried out, different LPG biosensors were used for this test and each transducer was used for the detection of two cumulative and consecutive analyte concentrations.

At the different concentrations (0.08 ng/mL, 0.88 ng/mL, 4.0 ng/mL, 8.0 ng/mL, 44 ng/mL and 88 ng/mL, corresponding to 0.12 pM, 1.2 pM, 6.0 pM, 12.1 pM, 60.1, 121.0 pM, respectively), we observed the following average values of $\Delta\lambda_{Tg\text{-}binding}$: 0.26 nm, 1.03 nm, 1.65 nm, 2.45 nm, 3.35 nm and 3.58 nm, respectively. A blank average value of 0.10 nm, accounting for the non-specific binding, was instead measured using the transducer without antibody coating. The corresponding dose-dependent curve is reported in Fig. 5, where we can observe the dose-dependency and the saturation reached yet between about 20 and 30 ng/mL of Tg (30.0 pM and 45.0 pM, respectively). Also, the analyte could be still detected with a remarkable difference over the non-specific recognition at the lowest concentration of 0.08 ng/mL (0.12 pM).

In order to uniform data obtained with different LPG biosensors, resonance shifts due to Tg capture were normalized based on Eq. (I). In particular each $\Delta\lambda_{Tg\text{-}binding}$ observed for Tg specific binding was normalized against the extent of antibody coating, expressed by $\Delta\lambda_{mAb\text{-}coating}$, achieved during the functionalization of the relative biosensor (See Eq. (I)). In fact, the two important variables affecting Tg quantification are antibody coating and probe sensitivity. Hydrophobic adsorption of the antibody can be influenced by several factors, such as temperature, exposure time, different surface properties and ligand orientation, thus influencing transducer sensitivity. Such variability could result in different effective detection capability and sensitivity between different functionalized biosensors. Moreover, any sensitivity variation of the biosensor associated to different polymer thickness, that could cause significant underestimation of Tg concentration, is in this way corrected. It is also important to underscore that the dip-coating technique used to deposit the polymer on the optical fibers, does not guarantee a tight control over polymer thickness at the nanometer scale. The normalization we have introduced attenuates the impact of such factors and we indeed observed an optimal correlation between data obtained with different optical fibers.

Data clearly show that human Tg bound with high affinity and in a dose dependent manner to the monoclonal antibody immobilized onto the solid phase. Also, it is worth noting that the level of nonspecific adsorption of analyte to the surface is particularly low, suggesting that functionalization and blocking were particularly effective and that selectivity was also particularly high, given the very poor recognition of albumin present at high concentration.

From the plot of resonance peak shifts against analyte concentration reported in Fig. 5, we also estimated a $K_D$ of about 6 pM, which is in the same low pM range of that determined by ELISA and by Biacore (about 70 pM). Such $K_D$ value also reflects the high sensitivity of the detection system, which is able to detect as low as 0.08 ng/mL Tg (0.12 pM) under these conditions. A linear dose–response is grossly obtained within the 0–4 ng/mL range (0–6.1 pM).

### 3.6. Quantification of Tg in clinical samples

RT-LPG-based biosensors were used for the *ex-vivo* detection of human Tg from needle washouts of fine-needle aspiration biopsies

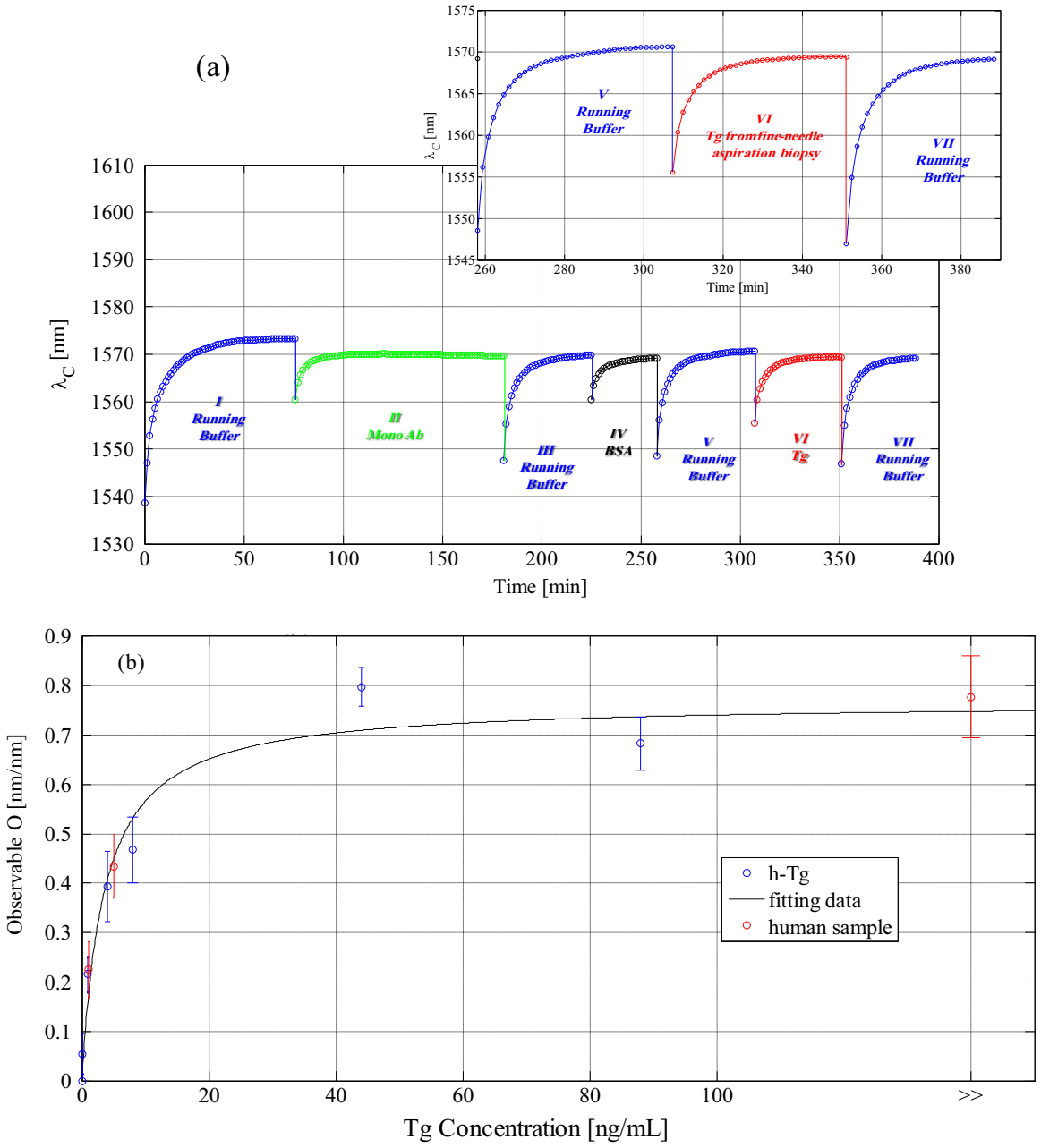


**Fig. 6.** (a) RT-LPG sensorgram reporting the wavelength shift of 6th order cladding mode attenuation band during human Thyrogobulin detection from the needle washout of fine-needle aspiration biopsy. In magnification the wavelength shift during Thyroglobulin binding event is reported. (b) Calibration curve for the semi-quantitative detection of human Thyroglobulin using RT-LPG biosensor and *ex-vivo* detection of human Thyroglobulin from needle washout of fine-needle aspiration biopsy. Blue dots refer to the dose-dependent assay performed to obtain the calibration curve, while red dots refer to the *ex-vivo* assay performed on human samples. The response is roughly linear within the range 0–4 ng/mL(0–6 pM). (For interpretation of the references to color in this figure legend, the reader is referred to the web version of this article.)

of thyroid nodules from several different patients. Fig. 6a shows typical sensorgrams obtained for such detection of human Tg. The transducer was functionalized as described above by immersing the probe in a solution containing the anti-Tg mAb. After the blocking step necessary to reduce non-specific adsorption of the analyte, the probe was immersed in solutions obtained by diluting the needle washout of fine-needle aspiration biopsies (steps V–VII in the magnification). Such solutions contained Tg at different concentrations, previously quantified using a standard immunoenzymatic assay. Different independent assays were performed with solution samples at increasing Tg concentrations, observing a remarkable correlation with the calibration curve previously obtained (Fig. 6b, red dots) and with the concentrations obtained by canonical Tg quantification. In particular, a first set of human samples was diluted at 1 ng/mL Tg (1.5 pM, within the linearly responsive range) and detection was performed with different RT-LPG biosensors. As shown in Fig. 6b, we obtained an average value for the observable *O* of 0.225 corresponding to 1.45 ng/mL Tg (2.2 pM), a value in very good agreement with the expected concentration. An independent detection assays were performed on human samples prepared at 5 ng/mL Tg (7.6 pM), obtaining average *O* values of 0.430, corresponding to 4.5 ng/mL (6.8 pM). Also in this case values were in an overall satisfactory agreement with those expected, confirming the linear dose–response within the expected range and, most importantly, the substantial lack of strong non-specific interactions with other high concentration plasma proteins that contaminate the washout samples. Finally, the detection assays were performed on

undiluted samples, coming from different patient specimens, having Tg concentrations higher than 3000 ng/mL (4.5 nM). The average *O* values obtained after Tg capture were 0.777, corresponding, as expected, to complete biosensor saturation. We reported the values on the plot of Fig. 6b as red dots after the dashed line to underline the substantial accordance between Tg detection with LPG biosensors and canonical immunoenzymatic techniques.

The measurement of Tg in the washout of the fine needle aspiration biopsy was initially proposed by Pacini et al., (1992) for early detection of neck lymph node metastases in patients with differentiated thyroid carcinomas. He reported that the levels of Tg detected in the aspirate, increases the reliability and specificity of fine needle biopsy. He reported also that fine needle aspiration biopsy-Tg detection had 100% sensitivity, whereas cytology produced 85% sensitivity. Cunha et al. in their study, also reported that fine needle aspiration biopsy-Tg detection was more sensitive than fine needle aspiration biopsy-cytology, in fact only 8 out of 17 recurrent patients were detected considering only the cytological report, whereas when combining the fine needle aspiration biopsy-cytology and fine needle aspiration biopsy-Tg detection, they attained a specificity and sensitivity of 100% with a diagnostic accuracy of 100% in the assessment of metastatic lymph nodes in thyroidectomized patients (Cunha et al., 2007). Remarkably, it is reported that the Tg warning cutoff level in fine needle aspiration biopsies is about 39 ng/mL (59 pM) in patients awaiting thyroid surgery and 1.1 ng/mL (1.7 pM) in patients after thyroid ablation (Frasoldati et al., 1999). Such reference values clearly indicate that the biosensor operates at best in a range of concentrations matching that having a high clinical relevance.

In order to improve prognosis of differentiated thyroid carcinomas, it is widely accepted that confirmed or suspected cervical LN metastases should be removed for local control. However either preoperatively with ultrasonography (US) or during the operation, it is difficult to recognize small and occult LN metastases in the central compartment (Chéreau et al., 2015). Although it is widely accepted that differentiated thyroid carcinoma recurrences after lymph node dissection is unrelated to the number of LNs removed (Albuja-Cruz et al., 2012), it is also well established that removing occult LN metastasis decreases the rate of recurrence in the neck (Roh et al., 2011). The clinical application of real time Tg detection will probably in a near future provide to surgeons a powerful and reliable tool to precisely identify metastatic lymph nodes.

## 4. Conclusions

For the first time, a fiber optic biosensor (specifically an LPG biosensor) has been used for Tyreoglobulin (Tg, cancer biomarker for metastatic lymph-nodes in patients affected by thyroid cancer) detection using a very specific antibody as biorecognition element. The study has been performed in case of synthetic Tg and extended to preliminary clinical tests using human sample to validate the platform.

Specifically, a reflection-type LPG biosensor, coated with a single layer of atactic polystyrene onto which a specific, high affinity anti-Tg antibody was adsorbed, allowed label-free detection of Tg in the needle washouts of fine-needle aspiration biopsies, at concentrations useful for pre- and post-operative assessment of the biomarker levels.

Analyte recognition and capture were confirmed with a parallel of on fiber ELISA-like assay, implemented here for the first time, using, in pilot tests, the biotinylated protein and HRP-labeled streptavidin for its detection.

Dose-dependent experiments showed that the detection is linearly dependent on concentration within the range between 0 and 4 ng/mL (0–6 pM), while antibody saturation occurs for higher protein levels. On the basis of our data, the RT-LPG biosensor coated with anti-Tg antibody as biorecognition element, demonstrated the capability to detect sub ng/ml concentrations of human Tg with limits of detection similar to or even lower than those provided by state of the art analytical instrumentation and kits, such as the Immulite 2000 Tg kit (Siemens Healthcare Diagnostic Products, UK) characterized by a functional sensitivity of 0.9 ng/mL (1.4 pM) and commonly used for Tg assays in clinical studies.

The good agreement obtained comparing tests obtained with recombinant and human samples indicates the high specificity of our fiber optic assay, which reflects the specificity and affinity of the antibody chosen as capturing bioreceptor. Indeed, the biosensor allowed the *ex-vivo* detection of sub ng/ml concentrations of human Tg from needle washouts of fine-needle aspiration biopsies of thyroid nodule from different patients. Although the times for the analysis are still in the hour range because of the limited uptake time required to stabilize coated LPGs when used in batch tests (Pilla et al., 2012a), the integration with a microfluidic system will significantly reduce the response time (Chiavaioli et al., 2014), making this method a valuable tool to be thoughtfully used in clinical studies.

Altogether, the data underline the high potential of the proposed biosensing platform and the several advantages of this kind of transducer: the absence of labeling requirements represents in fact an attractive alternative to traditional label-based techniques such as fluorescence, colorimetry or radioactivity-based approaches, without affecting the intrinsic affinity. Furthermore, it appears particularly useful for monitoring post-operative Tg levels, as the actual Tg warning concentration (about 1 ng/mL, 1.5 pM, mainly limited by immuno-assays precision) is well within our linear response range (about 0–4 ng/mL, 0–6 pM). We foresee that, following a further optimization (microfluidic integration to improve the response time and the control of antibody orientation to further enhance the sensitivity) and standardization of the detection protocol, such an application is close at hand under the current experimental settings. More importantly, fiber optic bioprobes, due to the peculiar geometrical features of optical fibers, intrinsically light-coupled platforms, could be easily integrated in medical needles and catheters (differently from other technological platforms) shifting the paradigm of bio-sensing toward *in vivo* operations. We, indeed, believe that a further engineering of the detection platform could allow the detection of Tg during biopsy collection, this would require suitable needles and proper microfluidic and washing devices for the removal of tissue debris and for analyte dilution. Addressing and facing the underlined issues will lead to new potential applications in precision medicine paving the way for new technology lines under the “Lab in a Needle” umbrella (Ricciardi et al., 2015).

## Acknowledgments

The authors gratefully acknowledge the financial support from the national project “Smart Health 2.0”, PON04a2_C funded by the Italian Ministry of Education, University and Research (MIUR) under the PON framework.

## References

Albuja-Cruz, M.B., Thorson, C.M., Allan, B.J., Lew, J.I., Rodgers, 2012. Surgery 152, 1177–1183.
Alwis, L., Sun, T., Grattan, K.T.V., 2013. Sens. Actuators B 178, 694–699.
Baldini, F., Brenci, M., Chiavaioli, F., Giannetti, A., Trono, C., 2012. Anal. Bioanal. Chem. 402, 109–116.
Brzozowska, E., Śmietana, M., Koba, M., Górska, S., Pawlik, K., Gamian, A., Bock, W.J., 2015. Biosens. Bioelectron. 67, 93–99.

Cao, J., Tu, M.H., Sun, T., Grattan, K.T.V., 2013. Sens. Actuators B 181, 611–619.
Chao, C.Y., Fung, W., Guo, L.J., 2006. IEEE J. Sel. Top. Quantum Electron. 12, 134–142.
Chen, X., Zhou, K., Zhang, L., Bennion, I., 2007. Appl. Opt. 46, 451–455.
Chéreau, N., Buffet, C., Trésallet, C., Tissier, F., Leenhardt, L., Menegaux, F., 2015. Surgery 15, 704–707.
Chiavaioli, F., Biswas, P., Trono, C., Bandyopadhyay, S., Giannetti, A., Tombelli, S., Basumallick, N., Dasgupta, K., Baldini, F., 2014. Biosens. Bioelectron. 60, 305–310.
Choi, S., Chae, J., 2009. Biosens. Bioelectron. 25, 118–123.
Chryssis, A.N., Saini, S.S., Lee, S.M., Yi, H., Bentley, W.E., Dagenais, M., 2005. IEEE J. Sel. Top. Quantum Electron. 11, 864–872.
Chung, J.W., Bernhardt, R., Pyun, J.C., 2006. Sens. Actuators B Chem. 118, 28–32.
Consales, M., Quero, G., Zuppolini, S., Sansone, L., Borriello, A., Giordano, M., Venturelli, A., Cusano, A., 2014. Proc. SPIE 9157, 23rd International Conference on Optical Fibre Sensors, 91575G.
Cunha, N., Rodrigues, F., Curado, F., Ilheu, O., Cruz, C., Naidenov, P., Rascao., M., Ganho, J., Gomes, I., Pereira, H., Real, O., Figueiredo, P., Campos, B., Valido, F., 2007. Eur. J. Endocrinol. 157, 101–107.
Cusano, A., Iadicicco, A., Pilla, P., Contessa, L., Campopiano, S., Cutolo, A., Giordano, M., 2006. Opt. Express 14, 19–34.
Dantham, V.R., Holler, S., Barbre, C., Keng, D., Kolchenko, V., Arnold, S., 2013. Nano Lett. 13, 3347–3351.
Del Villar, I., Matías, I.R., Arregui, F.J., Lalanne, P., 2005. Opt. Express 13, 56–69.
DeLisa, M.P., Zhang, Z., Shiloach, M., Pilevar, S., Davis, C.C., Sirkis, J.S., Bentley, W.E., 2000. Anal. Chem. 72, 2895–2900.
Eftimov, T., 2010. Applications of fiber gratings in chemical and biochemical sensing. In: Zourob, M., Lakhtakia, A. (Eds.), Optical Guided-Wave Chemical and Biosensors II, Springer Series on Chemical Sensors and Biosensors 8. Springer, Berlin, Heidelberg, pp. 151–176.
Endo, T., Kobayashi, T., 2011. Biochem. Biophys. Res. Commun. 416, 227–231.
Falate, R., Kamikawachi, R.C., Müller, M., Kalinowski, H.J., Fabris, J.L., 2005. Sens. Actuators B Chem. 105, 430–436.
Falciai, R., Mignani, A.G., Vannini, A., 2001. Sens. Actuators B Chem. 74, 74–77.
Fan, X., White, I.M., Shopova, S.I., Zhu, H., Suter, J.D., Sun, Y., 2008. Anal. Chim. Acta. 620, 8–26.
Frasoldati, A., Toschi, E., Zini, M., 1999. Thyroid 9, 105–111.
Garg, R., Tripathi, S.M., Thyagarajan, K., Bock, W.J., 2013. Sens. Actuators B 176, 1121–1127.
Giovanella, L., Bongiovanni, M., Trimboli, P., 2013. Curr. Opin. Oncol. 25, 6–13.
Hanumegowda, N.M., White, I.M., Oveys, H., Fan, X., 2005. Sens. Lett. 3, 315–319.
Hoa, X.D., Kirk, A.G., Tabrizian, M., 2007. Biosens. Bioelectron. 23, 15–160.
Huang, J., Lan, X., Kaur, A., Wang, H., Yuan, L., Xiao, H., 2013. Opt. Eng. 52, 014404.
James, S.W., Tatam, R.P., 2003. Meas. Sci. Technol. 14, R49–R61.
Ko, Y.S., Hwang, T.S., Han, H.S., Lim, S.D., Kim, W.S., Oh., S.Y., 2012. Pathol. Int. 62, 43–48.
Lee, M.R., Fauchet, P.M., 2007. Opt. Express 15, 4530–4535.
Magro, G., Perissinotto, D., Schiappacassi, M., et al., 2003. Am. J. Pathol. 163 (1), 183–196 2003.
Moon, J.H., Yong, I.K., Lim, J.A., Choi, H.S., Cho, S.W., Kim, K.W., Park, H.J., Paeng, J.C., Park, Y.J., Yi, K.H., Park, D.J., Kim, S.E., Chung, J.K., 2013. J. Clin. Endocrinol. Metab. 98, 1061–1068.
Pacini, F., Fugazzola, I., Lippi, F., Ceccarelli, C., Centoni, R., Miccoli, P., Elisei, R., Pinchera, A., 1992. J. Clin. Endocrinol. Metab. 74, 1401–1404.
Pacini, F., Pinchera, A., 1999. Biochimie 81, 463–467.
Pilla, P., Malachovská, V., Borriello, A., Buosciolo, A., Giordano, M., Ambrosio, L., Cutolo, A., Cusano, A., 2011. Opt. Express 19, 512–526.
Pilla, P., Manzillo, P., Malachovská, V., Buosciolo, A., Campopiano, S., Cutolo, A., Ambrosio, L., Giordano, M., Cusano, A., 2009. Opt. Express 17, 20039–20050.
Pilla, P., Sandomenico, A., Malachovská, V., Borriello, A., Giordano, M., Cutolo, A., Ruvo, M., Cusano, A., 2012a. Biosens. Bioelectron. 31, 486–491.
Pilla, P., Trono, C., Baldini, F., Chiavaioli, F., Giordano, M., Cusano, A., 2012b. Opt. Lett. 37, 4152–4154.
Ramachandran, S., Wang, Z., Yan, M., 2002. Opt. Lett. 27, 698–700.
Ren, H.C., Vollmer, F., Arnold, S., Libchaber, A., 2007. Opt. Express 15, 17410–17423.
Ricciardi, A., Crescitelli, A., Vaiano, P., Quero, G., Consales, M., Pisco, M., Esposito, E., Cusano, A., 2015. Analyst 140, 8068–8079.
Roh, J.L., Kim, J.M., Park, C.I., 2011. Ann. Surg. Oncol. 18, 1312–1318.
Schneider, B.H., Edwards, J.G., Hartman, N.F., 1997. Clin. Chem. 43, 1757–1763.
Skivesen, N., Tetu, A., Kristensen, M., Kjems, J., Frandsen, L.H., Borel, P.I., 2007. Opt. Express 15, 3169–3176.
Smietana, M., Koba, M., Brzozowska, E., Krogulski, K., Nakonieczny, J., Wachnicki, L., Mikulic, P., Godlewski, M., Bock, W.J., 2015. Opt. Express. 23, 8441–8453.
Spencer, C.A., Lopresti, J.S., 2008. Nat. Clin. Pract. 4, 223–233.
Teramura, Y., Iwata, H., 2007. Anal. Biochem. 365, 201–207.
Tornatore, L., Marasco, D., Dathan, N., Vitale, R.M., Benedetti., E., Papa., S., Franzoso, G., Ruvo, M., 2008. J Mol. Biol. 378, 97–111.
Tripathi, S.M., Bock, W.J., Mikulic, P., Chinnappan, R., Ng, A., Tolba, M., Zourob, M., 2012. Biosens. Bioelectron. 35, 308–312.
Website, ⟨http://www.neosensors.com⟩.
Weir, H.K., Thompson, T.D., Soman, A., Moller, B., Leadbetter, S., 2015. Cancer 121, 1827–1837.
Weisser, M., Tovar, G., Mittler-Neher, Knoll, S.W., Brosinger, F., Freimuth, H., Lacher, M., Ehrfeld, W., 1999. Biosens. Bioelectron. 14, 405–411.
Yin, Y., Li, Z.Y., Zhong, Z., Gates, B., Venkateswaran, S., 2002. J. Mater. Chem. 12, 522–527.
Zhang, Y., Shibru, H., Cooper, K.L., Wang, A., 2005. Opt. Lett. 30, 1021–1023.